# Multidimensional Study On The Corrosion Inhibition of Polypyrrole-Chitosan (PPy-CTS) Composites For Carbon Steel In Acid Medium

**Baiyi Chen**
Lanzhou University of Technology
**Guohe Xu**
Hebei Agricultural University
**Luyao Wang**
Lanzhou University of Technology
**Chen Zhang**
Lanzhou University of Technology
**Congcong Li**
Lanzhou University of Technology
**Guannan Ju**
Shandong University of Technology
**Huixia Feng** ( fenghx66@163.com )
Lanzhou University of Technology

**Research Article**

**Keywords:** acidic, corrosion, inhibition, physical

**Posted Date:** October 14th, 2021

**DOI:** https://doi.org/10.21203/rs.3.rs-958811/v1

# Abstract

The acidic corrosion of carbon steel is a great concern, which has caused serious economic losses on a global scale. Therefore, the exploitation of corrosion inhibition strategy for carbon steel and an in-depth study on its mechanism are of vital importance. Here we have developed a mixed type corrosion inhibitor of PPy-CTS, which incorporated the good solubility and adsorption capacity of chitosan (CTS) into the excellent corrosion inhibition performance of polypyrrole (PPy) by in-situ polymerization of pyrrole on CTS. The corrosion inhibition performance of PPy-CTS composites as a potential corrosion inhibitor for Q235 carbon steel in 1 M HCl solution was investigated by electrochemical (potentiodynamic polarization curve and AC impedance spectroscopy) and surface morphological (scanning electron microscopy and water droplet contact angle) characterization. The results revealed that PPy-CTS with the optimal concentration of 250 ppm achieved the highest corrosion inhibition efficiency of 91.1%. Subsequently, the corrosion inhibition mechanism was furtherly studied. Gibbs free energy obtained from the Langmuir isotherm model suggested that the absorption of PPy-CTS corrosion inhibitor on Q235 steel in 1 M HCl solution belonged to a combined type of physisorption and chemisorption, which resulted in the formation of a physical barrier preventing the carbon steel from corrosion. In addition, the conductive polymer PPy of corrosion inhibitor possessed an oxide-film anodic protection for carbon steel. Ultimately, PPy-CTS effectively suppressed the corrosion reaction of carbon steel in harsh acidic environment through the synergistic effect of physical barrier and anodic protection.


# Introduction

Carbon steel with excellent mechanical properties and low cost has been widely employed as a major part of engineering materials for petrochemistry, transportation, construction and medical industry [1–4]. However, the acid corrosion of carbon steel in harsh working environments has not only threatened people's life, but also caused enormous economic losses [5–7]. Therefore, a clear corrosion mechanism of carbon steel and corresponding effective corrosion inhibition strategy are highly desired. In recent years, conductive polymer coatings such as polypyrrole (PPy) and polyaniline (PANI) against corrosion of metals and alloys has received much attention [8,9]. Among these conductive polymers, PPy, as a commonly used conductive polymer, shows the advantages of low toxicity, easy fabrication, high conductivity and excellent environmental stability [8,10]. In addition to the physical barrier, which was employed as the mainly corrosion inhibition mechanism of the polymeric coatings, PPy possesses an anodic protection for metals through accelerating the firmly metal oxides layer formation and shifting its potential to the passive state [11–13]. Nevertheless, the applications of PPy as a corrosion inhibitor have been significantly limited by its poor dispersity in corrosive medium [14–16]. Therefore, it is essential to improve the molecular flexibility and water solubility of PPy-based corrosion inhibitor.

Chitosan (CTS), the only natural alkaline polysaccharide with rich nitrogen content, has been used as green corrosion inhibitor with the mechanism of physical barrier due to its inherent benefits, such as low cost, non-toxicity, good film-forming ability and so forth [17,18]. CTS has both a hydrophilic hydroxyl and an

amino that can provide coordination electrons, so that it could be quickly dispersed in the corrosive medium and tightly adsorbed to the metal surface forming a physical barrier. In this work, we incorporated the good solubility and adsorption capacity of CTS into the excellent corrosion inhibition performance of PPy by in-situ polymerization of pyrrole on CTS. Thus, PPy-CTS composite was obtained, which acted as a mixed type corrosion inhibitor with the synergistic effect of adsorption-film and oxide-film mechanism for carbon steel in acidic medium. PPy-CTS corrosion inhibitor could adsorb on the carbon steel surface rapidly at low content and achieve a stable corrosion inhibition effect, with the highest corrosion inhibition efficiency of 91.1%.

# Materials And Methods

## Materials

Q235 carbon steel (Western Region Supply Chain (Shanghai) Co., LTD，China), Chitosan (CTS) (Zhejiang Golden-Shell Biochemical Co., LTD., China), pyrrole (Py) (Aladdin reagent (Shanghai) Co., LTD., China), ammonium persulfate (APS) (Yantai Shuangshuang Chemical Co., LTD., China), anhydrous ethanol (Tianjin Damao Chemical Reagent Factory, China), acetone (Beijing Chemical Plant, China), hydrochloric acid (Baiyin Liangyou Chemical Reagent Factory, China).

## Methods

**Preparation of PPy-CTS corrosion inhibitor.** CTS powders was dispersed ultrasonic in 50 mL deionized water for 30 min. A certain amount of freshly steamed pyrrole (Py) monomer was quickly injected and stirred magnetic force at 5 ℃ for about 10 min until uniform dispersion. APS was dissolved in 10 mL deionized water in advance and slowly dropped into the above system for 10 min. After stirring for 6h at constant temperature, the reaction system was filtered. Ethanol and distilled water were used for washing successively. The filtrate residue was dried in a vacuum drying oven at 60 ℃ for 12 h to obtain the powdery PPy-CTS composite material.

**Fourier transform infrared spectroscopy (FT-IR) tests.** Fourier transform infrared spectrometer (NEXUS-470, Thermo Nicolet Co., LTD., America) was used for testing. The sample was dried and ground into powder, then mixed with KBr and pressed. The scanning range was 4000~800 $cm^{-1}$.

**X-ray diffraction (XRD) tests.** The samples were thoroughly dried and finely ground with an agate mortar and tested with an X-ray diffractometer (D8/ANDVANCE, BRUKER Co., LTD., Germany) with a CuKα radiation (λ=0.15418 nm) at 40 Kv and 40 mA at 25 ℃. The relative intensity was recorded in the scattering range of 5-50° at a scanning speed of 2°/min.

**Scanning electron microscope (SEM) tests.** SEM (JSM-6701F, Japan Electronics Optics Co., LTD., Japan) was used to observe the surface morphology of CTS, PPy, PPy-CTS and Q235 carbon steel with different corrosion.

**The treatment of Q235 carbon steel.** The size of Q235 carbon steel, as the corrosion test piece, was 10 mm×10 mm×3 mm. Before the test, seal the sample around with epoxy resin, leaving 1 $cm^2$ of exposed area. It was polished step by step with metallographic sandpaper (400#, 600#, 800#, 1200#, 1500#) until the surface was smooth and scratch free. Then, the surface was washed with distilled water, and ultrasonic cleaned with acetone and anhydrous ethanol for 10 min each.

**Electrochemical tests.** Electrochemical tests were performed on an electrochemical workstation (CHI660E, Shanghai Chenhua Instrument Co., LTD, China) using a three-electrode system at 298 K. Platinum plate was used as auxiliary electrode, saturated calomel electrode was used as reference electrode, and pre-treated carbon steel was used as working electrode. During the test, ensure that the effective contact area between the working electrode and the corrosive solution was 1 $cm^2$. The corrosive medium was HCl solution with a concentration of 1 mol/L.

For Tafel tests, the potential range was selected from -0.8 V to -0.1 V, and the scanning speed was 1 mV/s from cathode to anode. For EIS tests, at open circuit potential, frequency range was 0.01Hz ~ 10kHz, and ac excitation signal was 10mV. The data of AC impedance spectrum were fitted and analyzed by ZSimp Win.

Polarization resistance ($R_p$) was calculated by the following formula:

$$R_p = R_{ct} + R_f \quad (1)$$

In Equations 1, $R_{ct}$ and $R_f$ represented charge transfer resistance and membrane resistance.

Corrosion inhibition efficiency ($\eta$) was calculated by the following formula:

$$\eta = (i^0_{corr} - i_{corr}) / i^0_{corr} \times 100\% \quad (2)$$

$$\eta = (R_p - R^0_p) / R_p \times 100\% \quad (3)$$

In Equations 2 and 3, $i^0_{corr}$ and $i_{corr}$ represented the corrosion current density (A/$cm^2$) of Q235 carbon steel in HCl solution before and after the addition of corrosion inhibitor, respectively. $R^0_p$ and $R_p$ represented the polarization resistance (Ω•$cm^2$) of Q235 carbon steel in HCl solution before and after the addition of corrosion inhibitor, respectively.

**Energy dispersive X-ray spectrometer (EDS) tests.** The elemental analysis of surface of Q235 carbon steel with different corrosion was investigated using EDS (JSM-5600LV, Oxford Instruments Co., LTD., English).

**Contact angle (CA) tests.** Contact angle tester (SZ-CAMC33, Shanghai Xuanxun Instrument Co., LTD, China) was used to test the static CA of the sample surface. Drop 3μL of distilled water on the steel plate and take a picture with a digital camera.

# Results And Discussion

**Design and characterization of of PPy-CTS corrosion inhibitor.** Figure 1 has shown the acid corrosion and PPy-CTS corrosion inhibition on carbon steel. As can be seen in Fig. 1(a), the bare carbon steel can be easily corroded in acidic medium. This was because the Fe element in carbon steel lost electrons and was oxidized to $Fe^{2+/3+}$ by $H^+$, resulting in $H^+$ gaining electrons and being reduced to $H_2$. Finally, the $Fe^{2+/3+}$ dissolved from the metal surface. While, comparing with the corroded bare carbon steel, PPy-CTS acted as an efficient corrosion inhibitor and was chemically adsorbed on the carbon steel surface forming a polymeric coating and prevented the hydrogen ions in acidic medium from contacting the metal, thereby suppressing the corrosion reaction on the carbon steel. This was because that PPy-CTS could rapidly dissolve in the acidic medium owing to the favorable solubility of CTS, and then combined with the carbon steel firmly through the coordination bonds formed by the lone electron pair on adsorption centers like N and O of CTS and the empty orbital of the metal atom. In addition to the physical barrier, the $PPy^{n+}$ with strong oxidizing property has been widely used in anodic protection. It could oxidize the Fe elements and form a dense oxide layer on carbon steel surface, which passivated the carbon steel surface and achieved corrosion inhibition eventually.

CTS and pyrrole (Py) were used to synthesize the PPy-CTS composites simply and facilely with ammonium persulfate (APS) as an oxidant (Fig. 2(a)), which were eventually utilized as the corrosion inhibitor for carbon steel. (See Supporting Information for detailed steps.) To investigate the corrosion inhibition performance of PPy-CTS, its structure and morphology were characterized. In FT-IR analysis (Fig. 2(b)), it could be seen that the spectrum of PPy-CTS (iii) included the characteristic absorption bands from both PPy (i) and CTS (ii), which demonstrated the successful synthesis of PPy-CTS composites by one-step polymerization of Py grafting on CTS (Supporting Information Fig. S1) [19–21]. Figure 2(c) has shown the XRD patterns of PPy (i), CTS (ii) and PPy-CTS (iii). There were two sharp peaks at $2\theta = 12°$ and 20° in the pattern of CTS, which corresponded to the characteristic peaks of hydrated crystal structure [22] and regular (110, 040) lattice structure [23] of CTS, respectively. While, the PPy pattern showed a strong peak with the range from 16° to 28°, indicating the tightly arranged PPy molecular chains with a high order. In fact, the order of PPy molecular chain was directly related to its polymeric structure. When the polymerization temperature was low, the pyrrole monomers are mainly bonded into polymer chains in *α-α* way, and it was difficult to twist between the chain segments. As a result, the polymer chains tended to form a planar structure, which improved the order of PPy molecular chains. At the same time, the *π-π* conjugate system, which was very important for electron migration, also became more complete, and the conductivity of PPy increased relatively [24]. Remarkably, the pattern of PPy-CTS included the diffraction peaks belonging to CTS (10° and 19°) and PPy (15° ~ 27°). However, it was worth noting that, comparing with CTS and PPy, the peak positions of all peaks of PPy-CTS moved to the left, which was attributed to the successful graft of PPy on CTS [25]. Furtherly, the SEM images of CTS, PPy and PPy-CTS were given in Fig. 2(d). It can be observed that CTS possessed a relatively flat and tightly homogeneous surface, and PPy was consisted of regular spherical nano-scaled particles with the particle size of ~80 nm. After grafting PPy on CTS by one-step chemical oxidation method, the morphology of the composites revealed that the original smooth and flat CTS surface was evenly coated with PPy nano-scaled particles.

**Optimization of the PPy-CTS preparation conditions.** In order to investigate the corrosion inhibition performance of PPy-CTS, the preparation conditions of PPy-CTS corrosion inhibitor, such as the mass ratio of PPy/CTS and polymerization temperature, were optimized by electrochemical methods such as potentiodynamic polarization curve (Tafel) and AC impedance spectroscopy (EIS) (Fig. 3). Figure 3(a) and (b) showed the Tafel and EIS curves of Q235 carbon steel soaking in 1 M HCl corrosion solution containing corrosion inhibitor with different PPy/CTS mass ratios for 30 min, respectively. For Tafel tests, the cathodic and anodic polarization curves were similar, indicating that the change of PPy/CTS mass ratio in corrosion inhibitor did not affect the mechanism of cathodic hydrogen evolution and anodic metal dissolution reaction in the corrosion process of carbon steel. Similarly, for EIS analysis, Nyquist curves of all samples showed a single capacitive arc of approximately semi-circular shape, which also revealed the same corrosion mechanism. While, it was mentioned that the diameter of Nyquist curve first increased and then decreased with the increase of Py mass ratio, which corresponded to the opposite trend of corrosion current density ($I_{corr}$) (inset of Fig. 3(a)) during the corrosion of carbon steel. The decrease of $I_{corr}$ value indicated that the charge transfer intensity of metal surface in the corrosion solution was weakened, which was attributed to the dense protective layer forming by the corrosion inhibitor adsorbed on the metal surface. Consequently, the corrosion reaction was suppressed. Meanwhile, the polarization resistance ($R_p$) and corrosion inhibition efficiency ($\eta$) (Supporting Information Table S1 and S2) first increased and then decreased with the increase of Py mass ratio, which was contrary to the change of $I_{corr}$. When the mass ratio of Py to CTS was 0.1:1, the $I_{corr}$ was the minimum ($8.118\times10^{-4}$ A/cm$^2$), the $R_p$ and $\eta$ were the maximum (29.82 Ω·cm$^2$ and 85.57%, respectively), and the corrosion inhibition effect achieved the best. This was because the charge transfer direction in the redox reaction of PPy was opposite to that generated by the electrochemical corrosion of metal, which has significantly increased the charge transfer resistance and thus played a role in corrosion inhibition. However, as the mass ratio of Py increasing, the ratio of CTS decreased, which reduced the coordination bonds formed by the lone electron pair of the corrosion inhibitor with the metal atom, and thus the adsorption capacity of the corrosion inhibitor on the carbon steel surface decreased. Ultimately, the corrosion inhibition performance declined.

Figure 3(c) and (d) showed the Tafel and EIS curves of Q235 carbon steel soaking in 1 M HCl corrosion solution containing PPy-CTS corrosion inhibitor with different polymerization temperature for 30 min. For Tafel tests, the cathodic and anodic polarization curves with different polymerization temperature were similar, indicating that the change of polymerization temperature did not affect the mechanism of cathodic hydrogen evolution and anodic metal dissolution reaction in the corrosion process of carbon steel. For EIS analysis, Nyquist curves of all samples showed a single capacitive arc of approximately semi-circular shape, indicating the same corrosion mechanism. While, the diameter of Nyquist curve decreased with the increase of polymerization temperature, which corresponded to the opposite trend of corrosion current density ($I_{corr}$) and the same trend of $R_p$ and $\eta$ (Supporting Information Table S3 and S4) during the corrosion of carbon steel. This revealed that lower polymerization temperature was beneficial to improve corrosion inhibition ability of PPy-CTS. When the polymerization temperature was 5 ℃, the $I_{corr}$ was the minimum ($8.118\times10^{-4}$ A/cm$^2$), the $R_p$ and $\eta$ were the maximum (29.82 Ω·cm$^2$ and 85.57%,

respectively), and the corrosion inhibition effect achieved the best. As mentioned in XRD analysis, the effect of polymerization temperature on the corrosion inhibition efficiency of PPy-CTS was mainly due to the improvement of the order of PPy molecular chains and the π-π conjugation system at low temperature, and thus the conductivity of PPy increased relatively. As a result, the charge transfer ability of PPy was enhanced during the redox reaction, which has inhibited the transfer of corrosion charge, thus playing a role of electrochemical corrosion protection.

**The influence of concentration and soaking time on corrosion inhibition performance of PPy-CTS.** After determining the optimal preparation conditions of PPy-CTS corrosion inhibitor, the influence of corrosion inhibitor concentration and soaking time on the corrosion inhibition efficiency of PPy-CTS was studied, as shown in Fig. 4. Figure 4(a) and (b) showed the Tafel and EIS curves of Q235 carbon steel soaking in 1 M HCl corrosion solution with different PPy-CTS concentrations for 30 min. For Tafel tests, the anodic and cathodic polarization curves of all samples possessed the similar shapes. Meanwhile, all Nyquist curves showed the single capacitive arc with approximately semi-circular shape. This indicated that the concentration variation of PPy-CTS did not change the corrosion mechanism of carbon steel. However, comparing with the control group, the diameter of Nyquist curve increased significantly as the corrosion inhibitor concentration increasing, which reflected that the $I_{corr}$ decreased continuously and both the $R_p$ and $\eta$ showed the opposite (Table 1). This was because the adsorption active sites of PPy-CTS formed coordination bonds with the metal atom and generated an effective corrosion protection layer on the carbon steel surface, which could play a physical shield role and prevent the corrosive substances such as hydrogen ion, chloride ion and oxygen in the solution from contacting the metal. At the same time, the charge transfer during corrosion was inhibited by corrosion inhibitor. As the PPy-CTS concentration increasing, the charge transfer resistance ($R_{ct}$), $R_p$ and $I_{corr}$ increased, indicating the corrosion inhibition of carbon steel was enhanced. When the PPy-CTS concentration was 250 ppm, the $I_{corr}$ was the minimum and $\eta$ achieved the maximum (91.1%). In addition, comparing with the control group, the anodic and cathodic polarization curve slope ($\beta_a$, $\beta_c$) (Supporting Information Table S5) during corrosion reaction with corrosion inhibitor addition were both significantly increased, and the corrosion potential ($E_{corr}$) moved to the cathode. This revealed that PPy-CTS inhibited synchronously cathodic hydrogen evolution reaction and anodic metal dissolution reaction in the corrosion of carbon steel, and the cathode reaction was more inhibited than the anode reaction. Meanwhile, the displacement of Ecorr was less than 85 mV [26], indicating that PPy-CTS was a hybrid corrosion inhibitor. Therefore, as a hybrid corrosion inhibitor with cathodic inhibition as the mainstay [27], PPy-CTS had good corrosion inhibition effect.

Q235 carbon steel was soaked in the corrosive solution with 250 ppm corrosion inhibitor, and the influence of soaking time on corrosion inhibition efficiency was studied by EIS, as shown in Fig. 4(c). It could be seen from the figure that all Nyquist curves showed the single capacitive arc with approximately semi-circular shape with different soaking time (0.5-24 h). However, the diameter of Nyquist curve gradually decreased with the soaking time increasing, indicating that $I_{corr}$ increased correspondingly, while $R_p$ and $\eta$ decreased. Therefore, the corrosion inhibition efficiency of PPy-CTS gradually weakened with the soaking time increasing. As can be seen from Table 2, the $R_p$ decreased significantly after

soaking for 8 h, which was because that the adsorption rate of corrosion inhibitor on the carbon steel surface was gradually smaller than the desorption rate and the corrosion inhibitor coating gradually peeled off after 8 h. Finally, the corrosion inhibition efficiency decreased. And the gradual decrease of diffusion coefficient n also proved the peeling of the corrosion inhibitor coating [28,29]. However, the $\eta$ decreased from 91.1–78.6% after soaking for 24 h, indicating that PPy-CTS still maintained good corrosion inhibition efficiency.

Table 1
EIS fitting parameters of Q235 carbon steel in 1 M HCl solution with different PPy-CTS concentrations.

| Concentration (ppm) | $R_s$ ($\Omega \cdot cm^2$) | $Y_0 \times 10^{-4}$ ($s^n \Omega^{-1} \cdot cm^{-2}$) | $n$ (0<n<1) | $R_p$ ($\Omega \cdot cm^2$) | $\eta$ |
|---|---|---|---|---|---|
| 0 | 1.586 | 17.560 | 0.8623 | 4.411 | - |
| 50 | 1.570 | 1.841 | 0.8589 | 29.82 | 85.21% |
| 100 | 1.738 | 1.600 | 0.8567 | 35.66 | 87.63% |
| 150 | 1.611 | 1.626 | 0.8625 | 38.09 | 88.42% |
| 200 | 1.715 | 1.666 | 0.8581 | 43.25 | 89.80% |
| 250 | 1.681 | 1.538 | 0.8448 | 49.45 | 91.10% |

Table 2
EIS fitting parameters of Q235 carbon steel in 1 M HCl solution containing 250 ppm PPy-CTS for different soaking time.

| Soaking time (h) | $R_s$ ($\Omega \cdot cm^2$) | $Y_0 \times 10^{-4}$ ($s^n \Omega^{-1} \cdot cm^{-2}$) | $n$ (0<n<1) | $R_p$ ($\Omega \cdot cm^2$) | $\eta$ |
|---|---|---|---|---|---|
| 0.5 | 1.681 | 1.538 | 0.8448 | 49.45 | 91.10% |
| 1 | 1.579 | 1.734 | 0.8582 | 42.97 | 89.73% |
| 2 | 1.639 | 2.829 | 0.8516 | 41.36 | 89.34% |
| 4 | 1.674 | 4.528 | 0.8413 | 40.94 | 89.23% |
| 6 | 1.457 | 5.273 | 0.8589 | 40.48 | 89.10% |
| 8 | 1.517 | 7.091 | 0.8395 | 36.52 | 87.92% |
| 12 | 1.495 | 10.130 | 0.8237 | 28.65 | 84.60% |
| 24 | 1.453 | 18.860 | 0.8138 | 20.63 | 78.62% |

**The adsorption mechanism of PPy-CTS on carbon steel.** In order to furtherly study the inhibition mechanism of PPy-CTS, the surface coverage ($\theta$) was calculated through Tafel parameters and EIS fitting parameters, and then the concentration ($C$) and $\theta$ were substituted into the Langmuir adsorption isotherm model to study the interaction between PPy-CTS and Q235 carbon steel. Figure 4(d) presented the Langmuir adsorption isotherm curves fitted by Tafel (Fig. 4(d) top) and EIS (Fig. 4(d) bottom) of PPy-CTS on Q235 carbon steel surface at 298 K, and the fitting results were consistent. As shown in this figure, $C/\theta$ both had a linear relationship with $C$, that was, $C/\theta = C+1/K_{ads}$, and the regression coefficient $R^2$ was 0.99. The slopes of these two fitting lines were 1.079 (top) and 1.081 (bottom), both closed to 1.0. And the adsorption equilibrium constants $K_{ads}$ could be calculated as 168.1 L/g (top) and 170.6 L/g (bottom), respectively. The above results revealed that the PPy-CTS corrosion inhibitor was adsorbed on the carbon steel surface and formed a firmly monolayer protective coating [30], which has prevented the carbon steel from corrosion by $H^+$, $Cl^-$, oxygen and other corrosive substances effectively.
Following, by substituting the $K_{ads}$ into the formula $\Delta G_{ads}=-RT\ln(1000K_{ads})$ [31], the adsorption free energy ($\Delta G_{ads}$) of -29.81 kJ/mol (top) and -29.85 kJ/mol (bottom) were obtained, respectively. Since $\Delta G_{ads}<0$, it could be determined that the PPy-CTS molecules were spontaneously adsorbed on the carbon steel surface. At the same time, the $\Delta G_{ads}$ value obtained in our work lied between -20 and -40 kJ/mol, inferring that the absorption of PPy-CTS corrosion inhibitor on Q235 steel in 1 M HCl solution belonged to a combined type of physisorption and chemisorption [32].

**The evaluation of corrosion inhibition performance of PPy-CTS.** Furtherly, the morphology and water droplet contact angle (CA) of carbon steel surface before and after corrosion were measured to evaluate the corrosion inhibition performance of PPy-CTS, as shown in Fig. 5. SEM images, water droplet CA images and EDS analysis of bare carbon steel were given in Fig. 5(a). It can be seen that the bare carbon steel surface was flat and clear with only slight damage caused by traces of polishing with sandpaper. Fe and C were evenly distributed, while the content of O was very low (4.94%). The water droplet contact angle was about 68.5° indicating a clean and hydrophilic surface. After was soaking in 1 M HCl solution for 2 h, the carbon steel surface was significantly corroded and showed deep pits and cracks in SEM image (Fig. 5 (b)). The content of O on carbon steel surface increased (up to 11.45%), which was caused by the corrosion product $Fe_2O_3$. Meanwhile, water droplet spread on the corroded carbon steel surface with a contact angle of 41°, which were also attributed to the hydrophilic corrosion product $Fe_2O_3$. However, the carbon steel after soaking in 1 M HCl solution containing 250 ppm PPy-CTS was corroded slightly and showed relatively flat surface, without serious pitting, cracks and corrosion products. And the O content of 6.81% was mainly attributed to the dense iron oxides protective layer oxidized by the $PPy^{n+}$ with strong oxidizing property. Additionally, the N element appeared in the energy dispersive spectroscopy and showed the content of 2.38%, which was attributed to the adsorption of PPy-CTS corrosion inhibitor on carbon steel surface. The water droplet contact angle on this corrosion-resistant surface carbon steel increased obviously to 81.4°. This was mainly due to the hydrophobic PPy-CTS corrosion inhibitor coating, which prevented the corrosive solution from contacting the carbon steel thereby showing effectively corrosion inhibition performance.

Based on the above results, it can be inferred that the remarkable corrosion inhibition performance of PPy-CTS was attributed to the synergistic effect of the excellent film-forming ability of CTS and corrosion inhibition performance of PPy. The corrosion inhibition mechanism of PPy-CTS coating on carbon steel was shown in Fig. 5(d). In the corrosive environment, a corrosive galvanic cell could be constructed by the metal and the corrosive medium. When carbon steel was soaked in an acidic medium without corrosion inhibitor, Fe in carbon steel lost electrons and was oxidized to $Fe^{2+}$ by $H^+$. And then the $Fe^{2+}$ was dissolved from the surface of the metal. $Fe^{2+}$ was unstable and easily oxidized to $Fe^{3+}$. At the same time, $H^+$ gained electrons and was reduced to $H_2$. Over time, the carbon steel gradually corroded. When carbon steel was soaked in an acidic medium containing corrosion inhibitor, PPy-CTS was firmly adsorbed onto the carbon steel through the coordination bonds formed by the electron-rich hydroxyl and amino groups of CTS and metal atom. Meanwhile, the hydrophobic PPy chains faced outward, preventing $H^+$ from contacting the carbon steel. Furtherly, $PPy^{n+}$ with strong oxidative property, which acted as anodic protection, can intercept electrons of the metal surface and reduced. Thus, a dense oxides layer was formed, which increased the oxidation potential of metal. Consequently, PPy-CTS with the synergistic effect of physical barrier and anodic protection suppressed the corrosion reaction of carbon steel in harsh acidic environment.

# Conclusion

To sum up, we have prepared PPy-CTS composites as a corrosion inhibitor for carbon steel in acidic medium. The FT-IR and XRD analysis have demonstrated the corrosion inhibitor were successfully synthesized by in-situ polymerization of Py grafting on CTS. The corrosion inhibition performance of PPy-CTS for carbon steel in 1 M HCl solution was measured by electrochemical and surface morphological analysis approaches, which showed the highest corrosion inhibition efficiency of 91.1% with the optimal concentration of 250 ppm. Following, the corrosion inhibition mechanism was furtherly studied. According to the Langmuir adsorption isotherms, it can be concluded that PPy-CTS molecules were adsorbed on carbon steel through both physisorption and chemisorption interactions, which formed a physical barrier preventing the carbon steel from corrosion. In addition, the conductive polymer PPy of corrosion inhibitor possessed an oxide-film anodic protection for carbon steel. Therefore, the above results revealed that the PPy-CTS composites had great potentials for the carbon steel corrosion protection through the synergistic effect of physical barrier and anodic protection.

# Declarations


### Acknowledgements

This work was supported by the Natural Science Foundation of China (No. 21664009, 51063003 and 21902008), the Natural Science Foundation of China (No. 2020IM030400), and the Science and Technology Research Project of Higher Education in Hebei Province of China (supported by Education Department of Hebei Province，NO. BJ2017026).

### Author contributions

B.C. and G.X. performed the experimental procedures and wrote the manuscript text, H.F., B.C. and G.J. established the main idea and helped write the manuscript text, L.W. and C.Z. edited the manuscript text and helped perform the experiments, C.L. performed some experimental procedures and wrote a part of manuscript text.

### Competing interests

The authors declare no competing interests.

### Additional information

Correspondence and requests for materials should be addressed to H.F.

Reprints and permissions information is available at www.nature.com/reprints.

Publisher's note Springer Nature remains neutral with regard to jurisdictional claims in published maps and institutional affiliations.

## References

1 Rodríguez-prieto, A. *et al*. Fitness for service and reliability of materials for manufacturing components intended for demanding service conditions in the petrochemical industry. *IEEE Access* **8**, 92275-92286 (2020).

2 Burkle, D. *et al*. In situ SR-XRD study of FeCO3 precipitation kinetics onto carbon steel in CO2-containing environments: the influence of brine pH. *Electrochim. Acta* **255**, 127-144 (2017).

3 Drewniok, M.P., Campbell, J. & Orr, J. The lightest beam method-a methodology to find ultimate steel savings and reduce embodied carbon in steel framed buildings. *Structures* **27**, 687-701 (2020).

4 Xi, W.X. *et al*. Point-of-care antimicrobial coating protects orthopaedic implants from bacterial challenge. *Nat. Commun.* **12**, 5473 (2021).

5 Maurice, V. & Marcus, P. Progress in corrosion science at atomic and nanometric scales. *Prog. Mater. Sci.* **95**, 132-171 (2018).

6 Chen, H. *et al*. Effect of water flow on the microstructure, mechanical performance, and cracking susceptibility of underwater wet welded Q235 and E40 steel. *J. Mater. Process. Tech.* **277**, 116435 (2020).

7 Li, X. *et al*. Materials science: share corrosion data. *Nature* **527**, 441-442 (2015).

8 Zhu, Q. *et al*. Synergistic effect of polypyrrole functionalized graphene oxide and zinc phosphate for enhanced anticorrosion performance of epoxy coatings. *Compos. Part A Appl. Sci. Manuf.* **130**, 105752

(2020).

9 Zhu, X.M. *et al*. In-situ modulation of interactions between polyaniline and graphene oxide films to develop waterborne epoxy anticorrosion coatings. *Prog. Org. Coat.* **133**, 106-116 (2019).

10 Mao, J.F. *et al*. Conductive polymer waving in liquid nitrogen. *ACS Nano* **11**, 10409-10416 (2017).

11 Davoodi, A., Honarbakhsh, S. G. & Farzi, A. Evaluation of corrosion resistance of polypyrrole/functionalized multi-walled carbon nanotubes composite coatings on 60Cu-40Zn brass alloy. *Prog. Org. Coat*. **88**, 106-115 (2015).

12 Yao, W. *et al*. Superhydrophobic coatings for corrosion protection of magnesium alloys. *J. Mater. Sci. Tech.* **52**, 100-118 (2020).

13 Yao, Y. *et al*. Corrosion protection of epoxy coatings containing 2-hydroxyphosphonocarboxylic acid doped polyaniline nanofibers. *Prog. Org. Coat.* **139**, 105470 (2020).

14 He, Y.L. *et al*. A polypyrrole elastomer based on confined polymerization in a host polymer network for highly stretchable temperature and strain sensors. *Small* **14**, e1800394 (2018).

15 Wei, W.L. *et al*. Facile one-pot synthesis of well-defined coaxial sulfur/polypyrrole tubular nanocomposites as cathodes for long-cycling lithium-sulfur battery. *Nanoscale* **10**, 13037-13044 (2018).

16 Alizadeh, N. *et al*. Synthesis of highly fluorescent water-soluble polypyrrole for cell imaging and iodide ion sensing. *Anal. Chim. Acta* **1084**, 99-105 (2019).

17 Zhao, Y.F. *et al*. Poly(vinyl alcohol)-chitosan synthetic as a new type of highly efficient hemostatic sponge with blood-triggered swelling and high biocompatibility. *J. Mater. Chem. B* **7**, 1855-1866 (2019).

18 Lai, X. *et al*. Chitosan derivative corrosion inhibitor for aluminum alloy in sodium chloride solution: a green organic/inorganic hybrid. *Carbohyd. Polym.* **265**, 118074 (2021).

19 Chen, Y., Long, W. & Xu, H. Efficient removal of acid red 18 from aqueous solution by in-situ polymerization of polypyrrole-chitosan composites. *J. Mol. Liq.* **287**, 110888 (2019).

20 Ramasamy, P. *et al*. Extraction, characterization and antioxidant property of chitosan from cuttlebone sepia kobiensis (Hoyle 1885). *Int. J. Biol. Macromol.* **64**, 202-212 (2014).

21 Wang, J. *et al*. Synthesis and antimicrobial activity of Schiff base of chitosan and acylated chitosan. *J. Appl. Polym. Sci.* **123**, 3242-3247 (2012).

22 Li, D.H. *et al*. Synthesis, biodegradability and cytotoxicity of water-soluble isobutylchitosan. *Carbohyd. Polym.* **67**, 40-45 (2007).

23 Ali, A. *et al*. Structure and dynamics of polypyrrole/chitosan nanocomposites. *Polym. Int.* **67**, 1615-1628 (2018).

24 Chalmers, E. *et al*. Increasing the conductivity and adhesion of polypyrrole hydrogels with electropolymerized polydopamine. *Chem. Mater.* **32**, 234–244 (2020).

25 Manivasagan, P. *et al*. Multifunctional biocompatible chitosan-polypyrrole nanocomposites as novel agents for photoacoustic imaging-guided photothermal ablation of cancer. *Sci. Rep.* **7**, 43593 (2017).

26 Kong, P. *et al.* Polyaniline/chitosan as a corrosion inhibitor for mild steel in acidic medium. *RSC Adv.* **9**, 9211-9217 (2019).

27 Rikhari, B., Mani, S.P. & Rajendran, N. Electrochemical behavior of polypyrrole/chitosan composite coating on Ti metal for biomedical applications. *Carbohyd. Polym.* **189**, 126-137 (2018).

28 Li, X., Deng, S. & Fu, H. Benzyltrimethylammonium iodide as a corrosion inhibitor for steel in phosphoric acid produced by dihydrate wet method process. *Corros. Sci.* **53**, 664-670 (2011).

29 Bentiss, F., Lebrini, M. & Lagrenée, M. Thermodynamic characterization of metal dissolution and inhibitor adsorption processes in mild steel/2,5-bis(n-thienyl)-1,3,4-thiadiazoles/hydrochloric acid system. *Corros. Sci.* **47**, 2915-2931 (2005).

30 Lua, X.P. *et al*. Unveiling the inhibition mechanism of an effective inhibitor for AZ91 Mg alloy. *Corros. Sci.* **148**, 264-271 (2019).

31 Sığırcık, G., Yildirim, D. & Tüken, T. Synthesis and inhibitory effect of N,N'-bis(1-phenylethanol) ethylenediamine against steel corrosion in HCl media. *Corros. Sci.* **120**, 184-193 (2017).

32 Wang, X.M., Yang, H.Y. & Wang, F.H. An investigation of benzimidazole derivative as corrosion inhibitor for mild steel in different concentration HCl solutions. *Corros. Sci.* **53**, 113-121 (2011).

# Figures

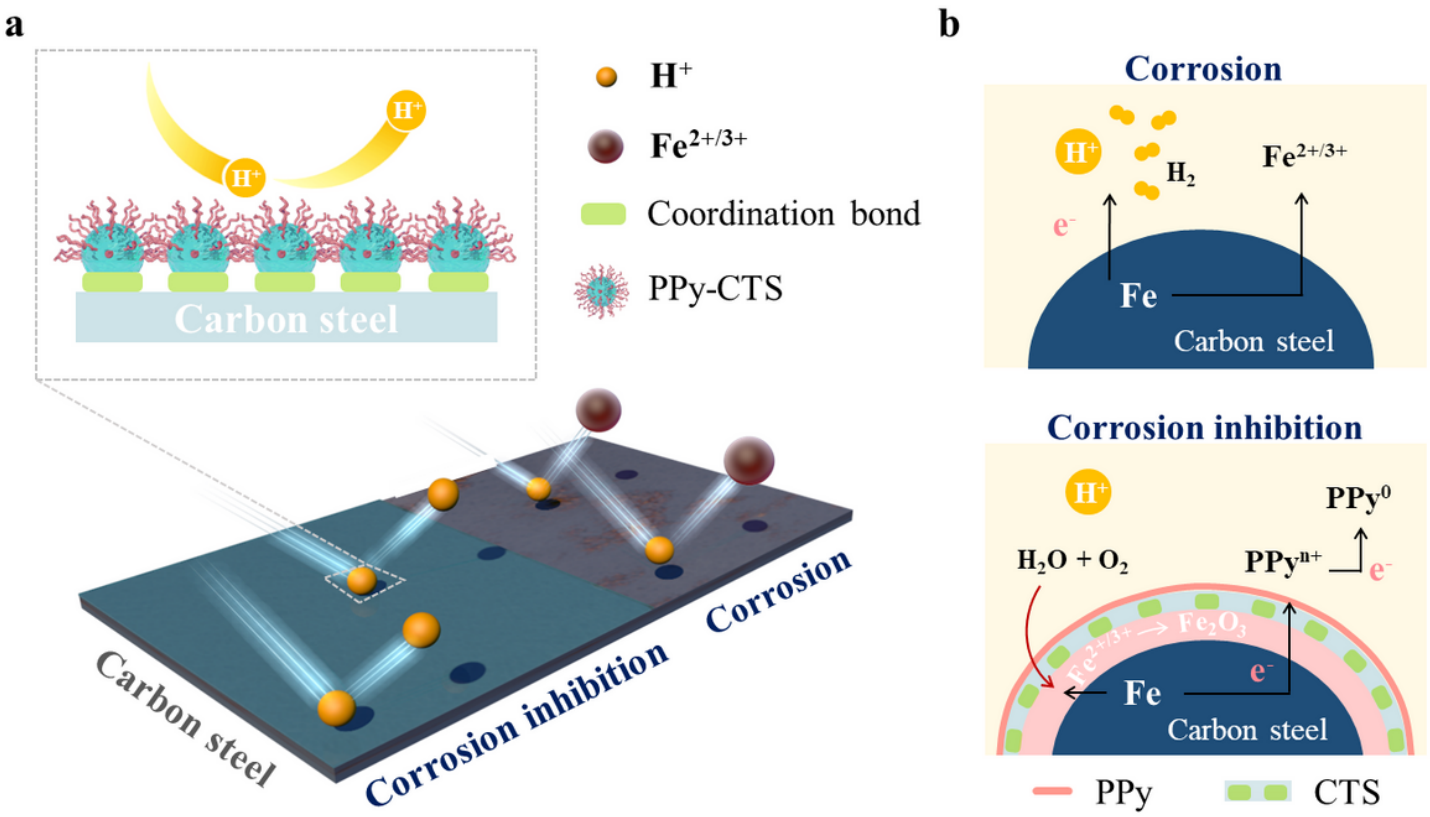


## Figure 1

Working principle of PPy-CTS corrosion inhibitor on carbon steel in acidic medium. PPy and CTS represent the polypyrrole and chitosan, respectively. The schematic diagram (a) and mechanism (b) of acid corrosion and PPy-CTS corrosion inhibition on carbon steel.

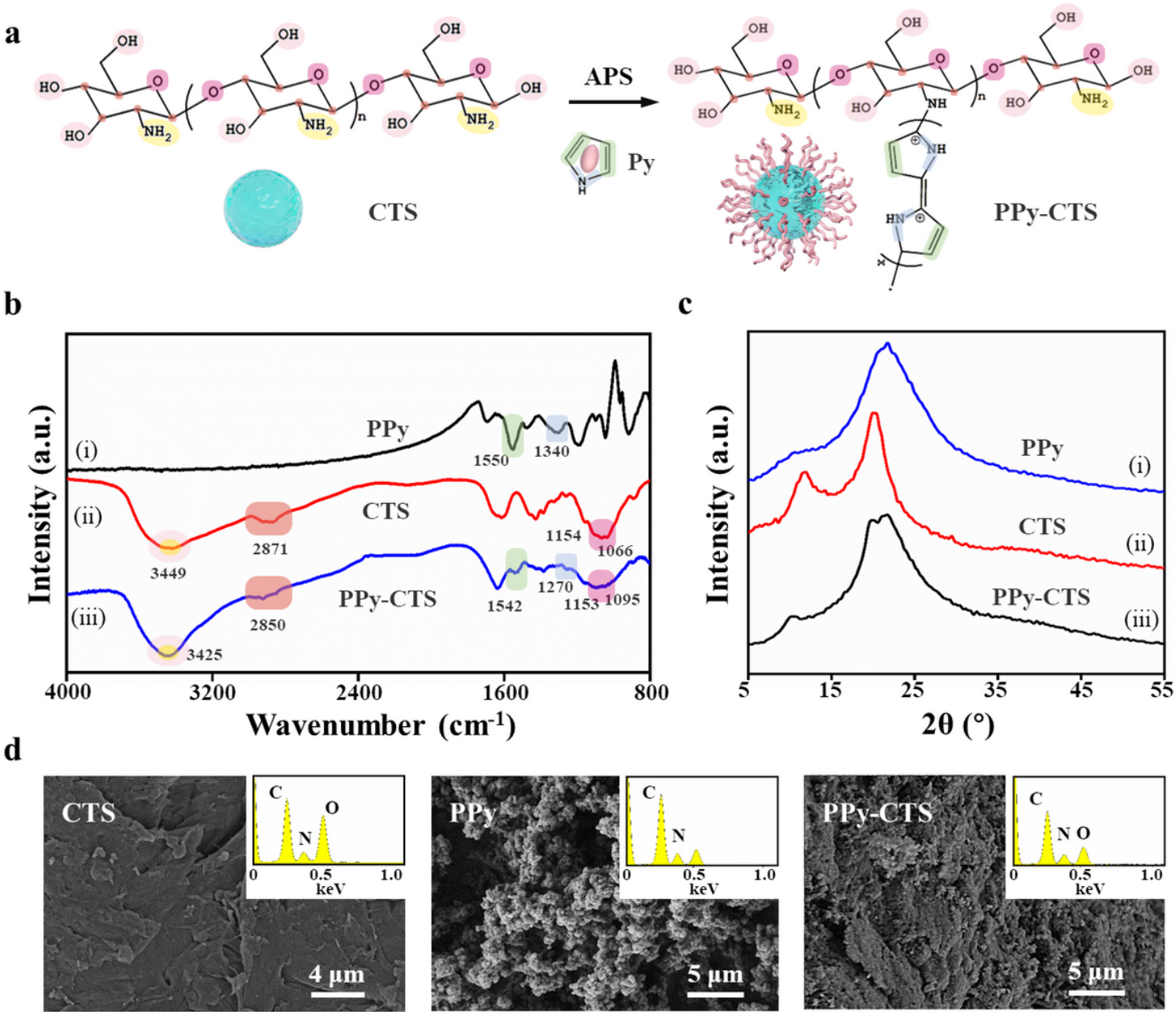


## Figure 2

Design and characterization of of PPy-CTS corrosion inhibitor. APS and Py represent the ammonium persulfate and pyrrole monomer, respectively. (a) The synthesis of PPy-CTS. (b) FT-IR spectra (left) and XRD patterns (right) of PPy, CTS and PPy-CTS. (c) SEM images and EDS analysis of CTS, PPy and PPy-CTS.

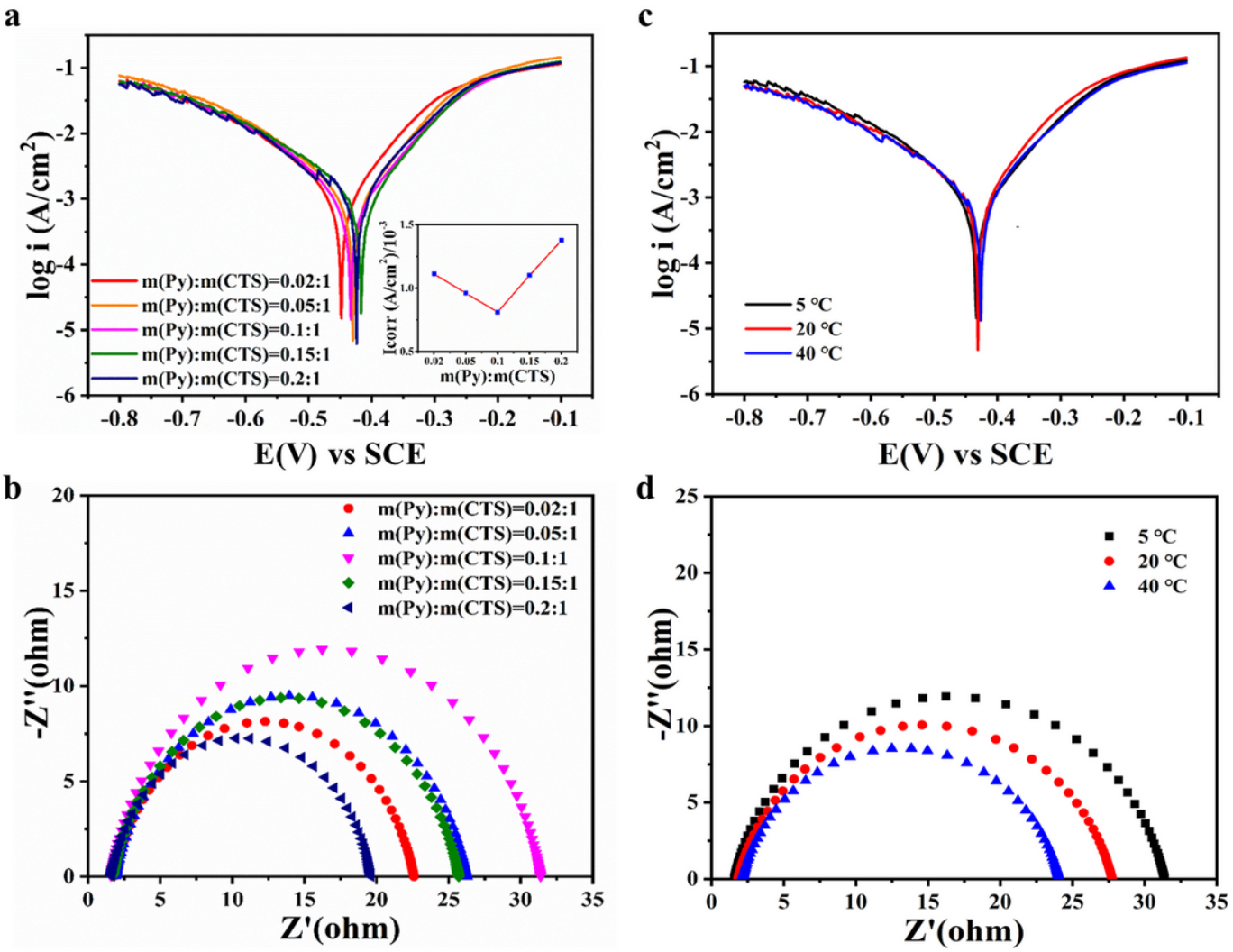


## Figure 3

Optimization of the PPy-CTS preparation conditions. Potentiodynamic polarization (a) and Nyquist (b) curves for Q235 carbon steel in 1 M HCl solution containing PPy-CTS corrosion inhibitor with different PPy/CTS mass ratio. Potentiodynamic polarization (c) and Nyquist (d) curves for Q235 carbon steel in 1 M HCl solution containing PPy-CTS corrosion inhibitor with different polymerization temperature.

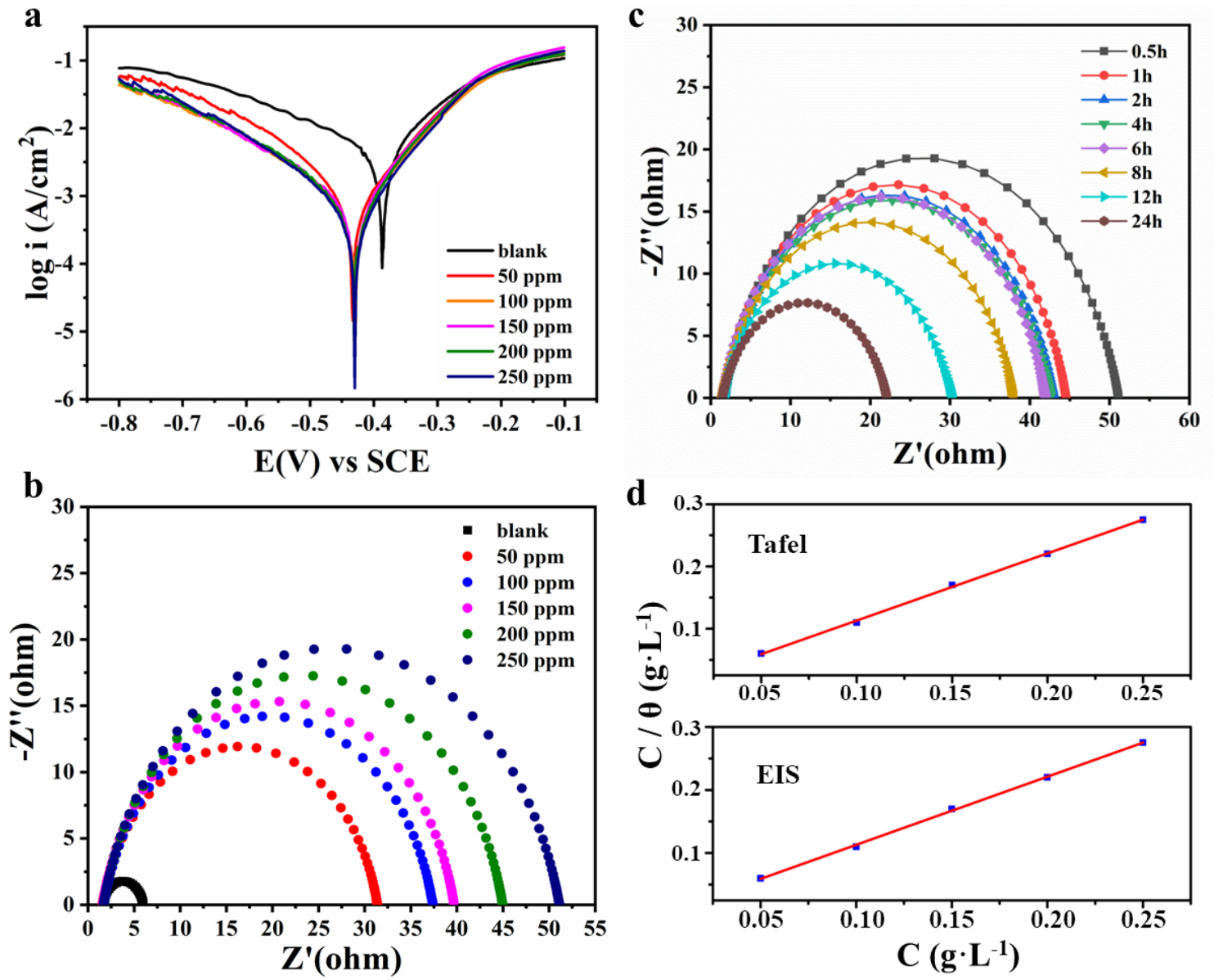


## Figure 4

The influence of concentration and soaking time on corrosion inhibition performance of PPy-CTS, and the adsorption mechanism of PPy-CTS on carbon steel. (a) Tafel and (b) Nyquist curves of Q235 carbon steel in 1 M HCl solution with different PPy-CTS concentrations for 30 min. (c) Nyquist curves of Q235 carbon steel in 1 M HCl solution containing 250 ppm PPy-CTS for different soaking time. (d) Langmuir adsorption isotherm curves fitted by Tafel (top) and EIS (bottom) of PPy-CTS on Q235 carbon steel surface at 298 K.

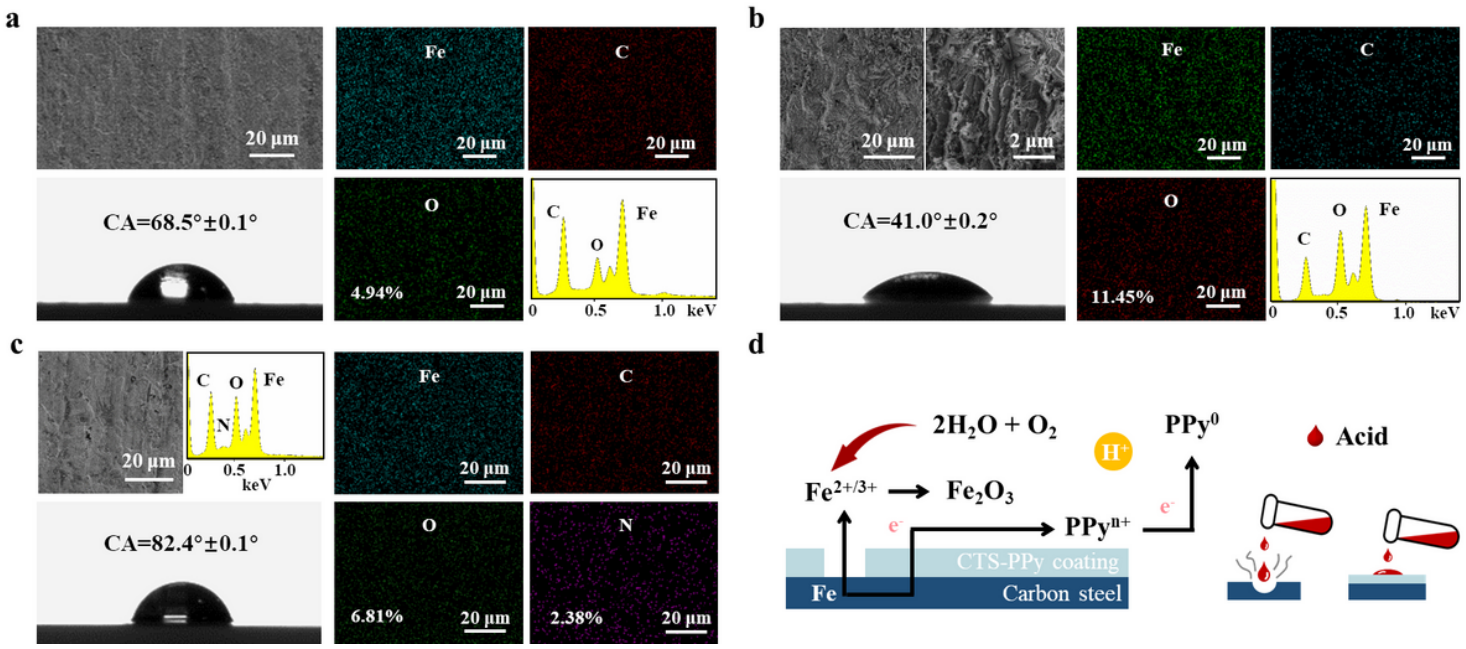


**Figure 5**

The evaluation of corrosion inhibition performance of PPy-CTS. SEM images, CA images and EDS analysis of (a) bare Q235 carbon steel, (b) Q235 carbon steel soaking in 1 M HCl solution for 2 h and (c) Q235 carbon steel soaking in 1 M HCl solution with 250 ppm PPy-CTS for 2 h. (d)The corrosion inhibition mechanism of PPy-CTS for carbon steel.

## Supplementary Files

This is a list of supplementary files associated with this preprint. Click to download.

- GraphicalAbstract.docx
- SupportingInformation.docx